BJR

https://doi.org/10.1259/bjr.20210220

Received: 12 February 2021 | Revised: 28 April 2021 | Accepted: 04 May 2021

Cite this article as:
Cannella R, Sartoris R, Grégory J, Garzelli L, Vilgrain V, Ronot M, et al. Quantitative magnetic resonance imaging for focal liver lesions: bridging the gap between research and clinical practice. *Br J Radiol* 2021; **94**: 20210220.

REVIEW ARTICLE

Quantitative magnetic resonance imaging for focal liver lesions: bridging the gap between research and clinical practice

[1,2,3]ROBERTO CANNELLA, MD, [1]RICCARDO SARTORIS, MD, [1,4]JULES GRÉGORY, MD, [1,4]LORENZO GARZELLI, MD, [1,4,5]VALÉRIE VILGRAIN, MD, PhD, [1,4,5]MAXIME RONOT, MD, PhD and [1,5]MARCO DIOGUARDI BURGIO, MD, PhD

[1]Service de Radiologie, Hôpital Beaujon, APHP.Nord, Clichy, France
[2]Section of Radiology - BiND, University Hospital "Paolo Giaccone", Via del Vespro 129, 90127 Palermo, Italy
[3]Department of Health Promotion Sciences Maternal and Infant Care, Internal Medicine and Medical Specialties, PROMISE, University of Palermo, 90127 Palermo, Italy
[4]Université de Paris, Paris, France
[5]INSERM U1149, CRI, Paris, France

Address correspondence to: Dr Maxime Ronot
E-mail: *maxime.ronot@aphp.fr*

ABSTRACT

Magnetic resonance imaging (MRI) is highly important for the detection, characterization, and follow-up of focal liver lesions. Several quantitative MRI-based methods have been proposed in addition to qualitative imaging interpretation to improve the diagnostic work-up and prognostics in patients with focal liver lesions. This includes DWI with apparent diffusion coefficient measurements, intravoxel incoherent motion, perfusion imaging, MR elastography, and radiomics. Multiple research studies have reported promising results with quantitative MRI methods in various clinical settings. Nevertheless, applications in everyday clinical practice are limited. This review describes the basic principles of quantitative MRI-based techniques and discusses the main current applications and limitations for the assessment of focal liver lesions.

INTRODUCTION

Focal liver lesions (FLLs) include a wide spectrum of benign and malignant tumors with different pathogeneses, clinical presentations, and outcomes. Magnetic resonance imaging (MRI) is extensively used as a non-invasive tool for the detection, characterization, assessment of treatment response, and follow-up of these lesions. In clinical practice, the assessment of FLLs is mainly based on the morphological and qualitative evaluation of MR images, including unenhanced sequences (T2W, in-phase, and opposed-phase sequences), dynamic imaging after the administration of a gadolinium-based contrast agent, and hepatobiliary phase imaging when a hepatobiliary contrast agent (*i.e.,* gadoxetate disodium or gadobenate dimeglumine) is administered.[1]

Characterization of FLLs is often challenging in clinical practice due to the overlap in imaging features among different types of tumors, atypical presentations, and uncommon tumor progression over time. Moreover, the qualitative assessment of imaging features is affected by the subjective interpretation of readers, different definitions of features among guidelines, and readers' experience, which can lead to suboptimal inter-reader agreement. The most challenging tasks for radiologists interpreting liver images include the differential diagnosis of FLLs, prediction of tumor aggressiveness or patient prognosis, and evaluation of treatment response after locoregional and systemic therapies.

In recent years, there has been growing interest in MRI-based quantitative methods to provide a more objective and reproducible assessment of FLLs. Theoretically, quantitative MRI could improve the diagnostic and prognostic accuracy when used in combination with conventional qualitative interpretations.[1] However, despite many promising research studies, only a few methods are actually used in routine practice for the assessment of FLLs. Certain techniques are frequently limited to their qualitative approach (*e.g.,* diffusion-weighed imaging with quantification of apparent diffusion coefficient [ADC]), while others are rarely used (*e.g.,* intravoxel incoherent motion, perfusion

imaging, MR elastography), or are still limited to the research field (*e.g.,* radiomics). This is confirmed by the absence of quantitative imaging methods in current clinical practice guidelines for the diagnosis and management of FLLs.

The purpose of this review is to describe the basic technical principles of several quantitative MRI-based techniques and to discuss the main current applications and limitations for the assessment of FLLs, placing the gap between research and practice into clinical perspective.

OVERVIEW OF THE MAIN QUANTITATIVE METHODS

Diffusion-weighted imaging

DWI provides qualitative and quantitative information based on the random movement of water molecules in human tissues. At present, DWI is integrated into the routine liver imaging protocol using Echo Planar Imaging (EPI) through modification of diffusion gradient strength and magnitude, represented by the *b*-value and measured in s/mm^2.[2] High *b*-values (>500 s/mm^2) provide key information on the restricted diffusion of water molecules. In tissues with low cellularity, such as cysts or necrotic areas, water protons have high freedom of movement and show a drop in signal intensity on high *b*-value DWI compared to low *b*-value DWI, while solid liver tumors (with high cellular density) restrict the diffusion of water protons and appear hyperintense on high *b*-value DWI.[3,4]

The acquisition of two or more *b*-values allows the point-by-point quantification of tissue diffusivity through the apparent diffusion coefficient (ADC) map, derived using a mono-exponential regression model.[5] The ADC map quantifies diffusion in each image voxel, expressed in 10^{-3} mm^2/s[5] (Table 1). In clinical practice, the quantitative assessment of diffusion can be easily extrapolated by drawing a region of interest (ROI) on the ADC map. Lesions with increased restricted diffusion will present low values on the corresponding ADC map.[3] DWI and the ADC map must be carefully compared in clinical practice. Some FLLs with long T2-relaxation times, such as hepatic hemangiomas, may present with persistent signal intensity on high *b*-value images, not because of increased restricted diffusion but due to the high signal intensity on T2W sequences that "shines through" to the high *b*-value DWI, mimicking a malignant lesion.[6] Thus, the ADC map makes it possible to differentiate true diffusion restriction from the T2 shine-through effect, since the latter will have high values on the corresponding ADC map.

Intravoxel incoherent motion

The DWI signal actually reflects a combination of water diffusion in tissue and perfusion-related effects due to the microcirculation in the normal capillary network.[7] Indeed, the liver is characterized by significant microperfusion with random movements of water molecules in blood capillaries within each image voxel, which constitute intravoxel incoherent motion (IVIM). The relative contribution of microperfusion and true diffusion-to-diffusion signal intensity is related to the *b*-value, with the weight of microperfusion being more significant at lower *b*-values.[7] IVIM analysis, presented by Le Bihan et al,[8] makes it possible to separate these two components by applying a bi-exponential model. IVIM analysis provides quantitative parameters that reflect both the diffusion of water molecules and regional microperfusion.[8] These parameters (Figure 1) include the true diffusion coefficient (D or D_{slow}), related to perfusion-free molecular diffusion restriction in tissue (the slow component of diffusion), pseudo-diffusion or perfusion-related diffusion (D* or D_{fast}), which is linked to microperfusion and incoherent motion of water molecules (fast component of perfusion), and the perfusion fraction (f), representing the fractional volume occupied by flowing spins in the voxel[5] (Table 1).

Perfusion imaging

Perfusion imaging is a quantitative technique that provides information about tissue microcirculation at levels below the spatial resolution of conventional imaging techniques.[9] In the liver, the most used approached is dynamic contrast-enhanced (DCE) MRI that requires i.v. gadolinium contrast administration as a tracer, followed by acquisition of signal-time curves that quantify changes in contrast concentrations over time.[4] Perfusion imaging acquisitions consist of free-breathing 3D perfusion sequences covering the entire liver with a short acquisition time (1–2 s) repeated for up to 5 min after contrast administration.[10] The main challenges of hepatic perfusion are related to the dual vascular supply of the liver (25% of perfusion from the hepatic artery and 75% from the portal vein), fenestrated sinusoids that allow rapid perfusion of the contrast agent and respiratory movements.[9]

DCE-MRI provides information based on the intralesional temporal distribution of contrast agents in lesions that often present with a heterogeneous vascular network. This is different from IVIM perfusion-related diffusion.[11] Lesion perfusion can be quantified by two major mathematical methods: a semi-quantitative approach, based on parameters reflecting the shape of time-intensity curves, and a quantitative approach, based on pharmacokinetic models reflecting changes in contrast agent concentrations. Parameters that are often analyzed by the semi-quantitative approach include the the time-to-peak enhancement (TTP; defined as the time between arrival of the tracer and maximum enhancement), area under the curve (amount of enhancement during a specific time interval), maximum enhancement (peak height), and maximum slope (Table 1). Although these are the most widely adopted semi-quantitative parameters, they are affected by acquisition parameters, injection protocols including contrast volume and injection rate, and physiological conditions such as respiratory motion.[1]

Quantitative models *per se* rely on the change in concentrations of the contrast agent using pharmacokinetic modeling techniques. Unlike the hepatic parenchyma, most liver tumors have mainly arterial input and no or low portal venous blood supply, which may be best analyzed using single-input models. Dual-compartment models such as the Kety or Tofts and the extended Kety models are the most frequently used.[12] In the Kety model, the transfer constant between plasma and the extravascular extracellular space (K^{trans}) and the extravascular extracellular volume

Table 1. Main quantitative MRI methods for the assessment of focal liver lesions.

Methods and Parameters	Definition	Biological correlate
Diffusion-weighted imaging		
Apparent diffusion coefficient (mean, min, max)	Quantification of tissue diffusivity (10^{-3} mm^2/s)	Tissue cellularity &
Apparent diffusion coefficient ratio	Ratio between lesion and liver parenchyma apparent diffusion coefficients	architecture
Intravoxel incoherent motion		
D or D_{slow}	Perfusion-free molecular diffusion restriction (10^{-3} mm^2/s)	Tissue cellularity & architecture
Da or D_{fast}	Perfusion-related diffusion (10^{-3} mm^2/s)	Microperfusion
Perfusion fraction (f)	Fractional volume occupied by flowing spins in the voxel (%)	% of perfusion
Dynamic contrast-enhanced MRIa		
Semi-quantitative parameters		
Area under the curve	Amount of enhancement during a specific time interval (dimensionless)	
Maximum slope	Slope of enhancement (dimensionless)	
Maximum enhancement	Peak height (dimensionless)	
Time-to-peak enhancement	Time between arrival of the tracer and maximum enhancement (s)	
Quantitative models		Tissue microcirculation
Perfusion	Quantification of tissue perfusion (mL/s/g)	
Blood volume	Quantification of volume of blood (mL/g)	
Blood flow	Quantification of flow of blood (mL/s)	
K^{trans}	Transfer constant between plasma and the extravascular extracellular space (s^{-1})	
v_e	Extravascular extracellular volume (%)	
v_p	Fractional plasma volume (%)	
MR elastography		
Stiffness	Quantification of the of the resistance offered to deformation (kPa)	
Viscosity	Quantification of the resistance to deformation at a given rate (Pa.s)	
Dynamic modulus G	Ratio of stress to strain under vibratory conditions (kPa)	Tissue shear properties
Storage modulus G'	Represents stored energy, related to elasticity (kPa)	
Loss modulus G"	Represents dissipated energy, related to viscosity (kPa)	
Radiomicsa		
First order features		
Mean	Average of the pixels within the ROI	
Standard deviation	Dispersion from the mean	
Skewness	Asymmetric of the histogram	
Kurtosis	Peakedness/flatness of the histogram	
Entropy	Image irregularity or complexity	
Second order features		Tissue heterogeneity

(Continued)

Table 1. (Continued)

Methods and Parameters	Definition	Biological correlate
Grey level co-occurrence matrix	Arrangements of pairs of pixels with the same values in specific directions	
Grey-level run length matrix	Consecutive pixels with the same intensity along specific directions	
Gray-level zone length matrix	Size of homogeneous zones for each gray-level in multiple dimensions	
Neighborhood gray-level different matrix		
Third order features		
Laplacian of Gaussian spatial band-pass filter	Highlights image features of different sizes corresponding to the spatial scale of the filter	
Wavelet transform	Evaluates spatial location of image features in addition to their frequency characteristics	

[a]The provided list is not exhaustive.

Figure 1. Example of intravoxel incoherent motion DWI with 10 *b*-values (ranging from *b* 0 to *b* 800), parametric maps of D, D*, f, and logarithmic plot of biexponential signal decay curve (red curve) and fitting curve (blue curve) in a 65-year-old patient with hepatocellular carcinoma developed on HCV-related cirrhosis.

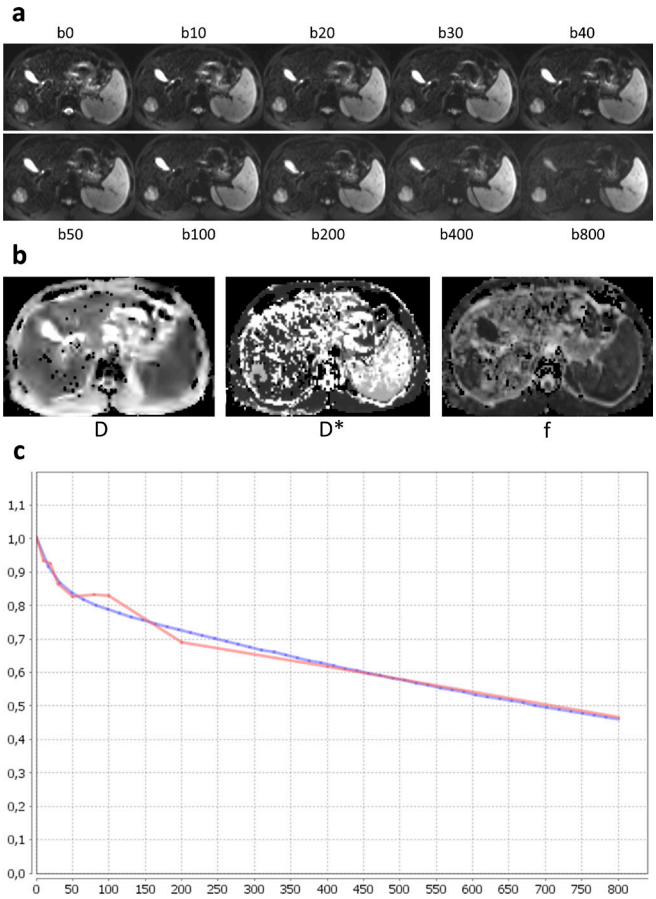

(v_e, %) are calculated. In the extended Katy model K^{trans}, v_e, and the fractional plasma volume (v_p, %) are assessed (Table 1).

Elastography

Magnetic resonance elastography (MRE) quantifies the mechanical properties of tissues by measuring the propagation of shear waves induced by an external vibrating compression device.[13,14] The external driver generates a continuous acoustic vibration that is transmitted throughout the entire abdomen.[14] MRE images are acquired using a phase-contrast pulse sequence with motion-encoding gradients synchronized to the mechanical waves.[13,14] This sequence detects the shear waves that are converted in quantitative maps (known as elastograms) of tissue stiffness (measured in kPa by drawing region of interests) and colored elastograms used for qualitative interpretation. Other mechanical properties such as tissue viscosity may be assessed (Table 1).

Radiomics

Radiomics is a new quantitative method that extracts a large number of mathematical features that cannot be assessed visually.[15] Radiomic features quantify the distribution of signal intensities within an ROI reflecting lesion heterogeneity.[16] Therefore, it is not an MR quantitative methods *per se*, but rather a quantitative approach that can be applied to MRI. Indeed, radiomics was initially applied to CT imaging, but experimental applications are rapidly expanding to MRI and can be theoretically performed in all MRI sequences.[17] The radiomic workflow involves a complex multistep process including imaging acquisition, lesion segmentation, feature extraction, reduction and selection, model building, and finally validation in internal and external cohorts.[18] Lesion segmentation (Figure 2) and feature extraction are the most critical steps. Several in-house designed, commercially available, or open-source research softwares have been used for lesion segmentation using manual, semi-automatic, or automatic tools. Although manual segmentation by expert radiologists is still considered to be the gold standard,

Figure 2. 68-year-old male with HBV cirrhosis. Contrast-enhanced MRI on hepatic arterial (A), portal venous (B), and delayed (C) phases shows a 33-mm hepatocellular carcinoma with arterial phase hyperenhancement (A), washout and capsule (B and C). Tumor segmentation (D) was performed on portal venous phase by manually drawing a region of interest within the lesions margin, using a freely available software (LIFEx, www.lifexsoft.org). Corresponding histogram (E) shows distribution of signal intensities within the region of interest.

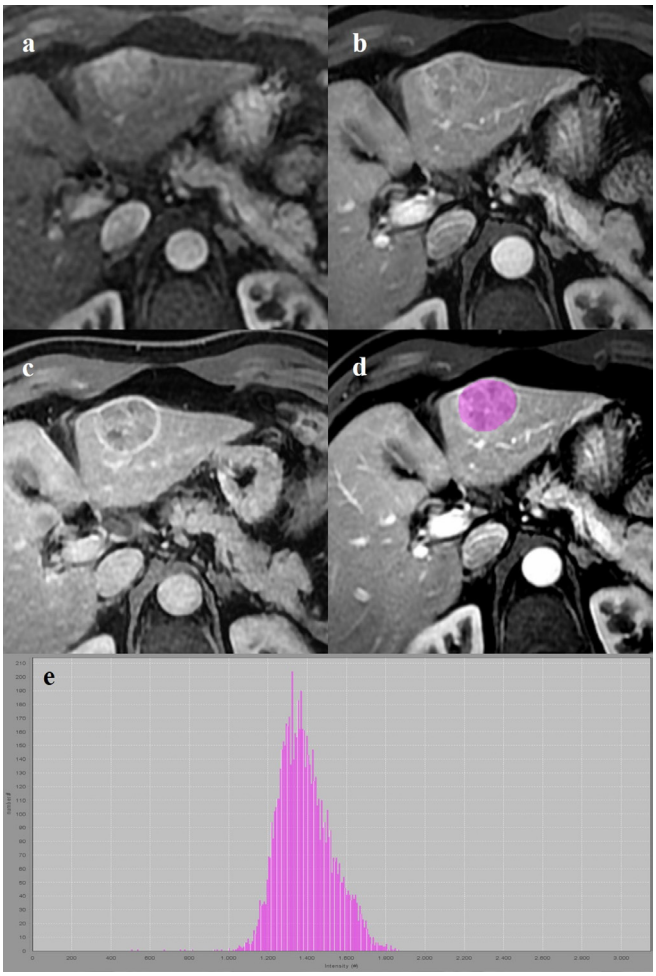

this is time-consuming and may be affected by intra- and inter-reader variability.[19] Segmentation of FLLs is usually obtained by drawing an ROI on the largest lesion cross-section or a 3D ROI on the whole lesion. A large number of quantitative mathematical features are then extracted. First-, second-, and third-order radiomic features are then classified (Table 1).[18,19]

APPLICATIONS IN FOCAL LIVER LESIONS: RESULTS AND PERFORMANCE

Tumor detection and characterization

One should keep in mind that the performance of qualitative and visual analysis of MR imaging for the detection and characterization of focal lesions is very high. Therefore, the added value of quantitative methods is expected to be limited.

Figure 3. 44-year-old male with chronic hepatitis B and two liver lesions on T2W image (A) and contrast-enhanced MRI (B) consistent with hepatocellular carcinoma (arrows) and hepatic hemangioma (arrowheads). On diffusion-weighted imaging (C), both lesions demonstrate high signal intensities at *b* 800. On apparent diffusion coefficient (ADC) map (D), mean value of hepatocellular carcinoma was 771 mm^2/s in the most restricted tumor area, while no diffusion restriction was observed in hepatic hemangioma (mean ADC value of 1746 mm^2/s).

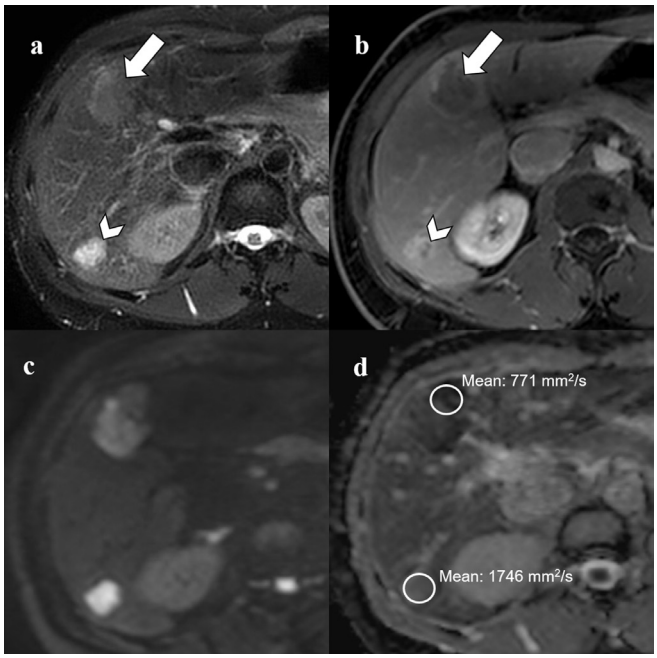

Diffusion-weighted imaging

DWI is by far the most widely used technique, routinely included in clinical practice. It has been shown to be more sensitive for the detection of FLLs than other MRI sequences. The main advantage of DWI is that it is rapidly acquired with no need for i.v. contrast administration. Nevertheless, and noticeably, the vast majority of published studies use a strict qualitative visual assessment of ADC in FLLs (*i.e.*, hypersignal intensity on high *b*-value or not).

Quantitative measurements are less routinely performed and reported in clinical practice than qualitative assessments. Historically, ADC values have been extensively studied for the discrimination between benign and malignant FLLs. Hepatic cysts and hemangiomas have been shown to have significantly higher ADC values than non-cystic malignant FLLs, and malignant tumors to have ADC values lower than that of the liver (Figure 3).[20] In our opinion, this benign/malignant opposition is frequently clinically irrelevant, and misleading. It does not reflect the management of patients with liver lesions and does not take into account the clinical context.

For instance, in patients with fortuitously discovered lesions, the vast majority of lesions are benign but may require dramatically different treatments. In one retrospective study, focal nodular hyperplasia and hepatocellular adenoma, which are two benign hepatocellular tumors with different management strategies,

were shown to have lower ADC values than the background liver parenchyma, and ADC was of limited help for the differentiation between the two entities.[21]

Furthermore, ACD measurements are known to be affected by the type of MR scanner and field strength. The ratio between lesions and background parenchyma ADC values has been proposed in some studies to improve the accuracy of the differential diagnosis, with a slightly higher reported accuracy than standard ADC values (92% *vs* 89%).[22] In patients with cirrhosis, it has been used to differentiate low-grade (LGDN), high-grade dysplastic nodules (HGDN) and hepatocellular carcinoma (HCC). In the study by Inchingolo et al, the sensitivity, specificity, and accuracy for the diagnosis of "HCC +HGDN" were 90.9%, 81.0%, and 83.6%, respectively, when lesion-to-liver ratio was <0.95.[23]

Mean or minimum ADC values have also been evaluated according to different histopathological features of HCC, with histopathological differentiation of HCC showing inverse correlation with the ADC value ($r = -0.51$, $p = 0.012$).[24] In line with these results, Li et al. reported a sensitivity of 69.6% and a specificity of 73.4% of mean ADC for the differentiation between poorly and non-poorly differentiated HCC (with a cutoff value of 0.96×10^{-3} mm^2/s) and a sensitivity of 78.3% and a specificity of 61.5% of minimum ADC (with a cutoff value of 0.90×10^{-3} mm^2/s).[25] This was expanded by Ogihara et al. using a multivendor approach.[26] Finally, Zhao et al, in a large retrospective study, showed a significantly lower ADC values in HCC with microvascular invasion (MVI) on histopathology.[27] The mean ADC provided a sensitivity of 79.2% and a specificity of 50.5% (with a cut-off value of 1.19 × 10 mm/s) for the identification of MVI.

Intravoxel incoherent motion

The performance of IVIM parameters for the characterization of FLLs has been assessed in several studies. The true diffusion coefficient (D) of benign FLLs, such as cysts and hemangiomas, was shown to be significantly higher than in primary and secondary malignant tumors, while results on the performance of perfusion-related diffusion (D*) and the perfusion fraction (f) are discordant.[28–32] So far, the added value of IVIM over ADC does not seem to be major. There is even a trend toward a better performance of ADC values in some studies to differentiate benign and malignant FLLs.[31–34]

IVIM parameters have been also evaluated for the prediction of histopathological grade with studies showing that high-grade HCCs have significantly lower D and ADC values than low-grade tumors.[35–38] A recent meta-analysis including 16 studies concluded that both ADC and D are highly accurate for the non-invasive grading of HCC with pooled sensitivity and specificity of the ADC value and D for the discrimination of poorly differentiated HCC of 84 and 80%, and 92 and 77%, respectively.[39] D was only better for the prediction of poorly differentiated HCC (AUROC was 0.94 for D *vs* 0.89 for ADC, $p = 0.007$).[39] Low D values have also been identified in HCC with MVI (AUROC of 0.815 (95% CI, 0.740–0.877), while no differences were observed in IVIM perfusion parameters.[40,41]

Finally, IVIM parameters have been correlated with histopathology and genetic expression of resected colorectal liver metastases. Granata et al. suggested that the diffusion coefficient (AUROC 0.80) and diffusional kurtosis (a measure of the "tailedness" of the distribution) (AUROC 0.80) could help predict the presence of Kras mutation[42] while Chiaradia et al[43] reported that both D ($r = 0.36$; $p = 0.035$) and ADC values ($r = 0.4$; $p = 0.02$) were correlated with the degree of tumor necrosis in metastases, but not with that of viable tumor.

Perfusion imaging

There are very few studies of MRI perfusion parameters for the characterization of liver tumors. Certain studies show that semi-quantitative perfusion parameters from multiphase dynamic contrast-enhanced MR differ between hemangioma and malignant tumors (*i.e.,* HCC, cholangiocarcinoma and metastases).[44,45]

Studies have shown that both HCC and liiver metastases and HCC can be differentiated using perfusion and permeability parameters extracted from perfusion MR sequences.[46,47] Similarly, authors reported on ability of distribution volume and perfusion to differentiate liver metastases from neuroendocrine tumors according to their enhancement pattern (*i.e.,* hypo or hyperenhanced).[48]

In cirrhotic patients, most studies have focued on the differentiation between benign dysplastic nodules and HCC. Authors have shown that both the arterial fraction and the arterial hepatic blood flow were significantly higher in HCC. The portal venous blood flow and the distribution volume were found significantly lower in HCC compared to the surrounding cirrhotic parenchyma, likely due to significant changes in tumor microvascular architecture and angiogenesis.[49]

Liver metastases induce changes in local hepatic hemodynamic (*e.g.,* decrease in portal venous perfusion, or increase in arterial perfusion that were historically documented by CT and hepatic scintigraphy. More recently, studies using perfusion MRI were able to replicate these results.[50] The clinical implication of such studies remain very limited since secondary tumors were already depicted on morphological cross-sectional imaging modalities.

Elastography

There are only a few reports on tumor stiffness quantification for the characterization of FLLs. Initial studies reported significantly greater stiffness in malignant FLLs than in benign tumors, with the greatest stiffness in intrahepatic cholangiocarcinoma due to abundant intralesional desmoplastic stroma. A cutoff value of 5 kPa was proposed in a preliminary study by Venkatesh et al. to accurately differentiate benign from malignant FLLs.[51] Another study analyzed MRE-based viscoelastic parameters for the characterizations of FLLs showing significantly higher stiffness in HCC than in benign hepatocellular tumors.[52] Preliminary data also reported a correlation between HCC tumor stiffness (Figure 4) and the grade of HCC, with a trend toward increased tumor stiffness in well/moderately differentiated HCCs (6.5 ± 1.2 kPa; $n = 13$) compared to poorly differentiated HCCs (4.9 ± 1.2 kPa; $n = 8$, $p < 0.01$).[53] Finally, ongoing research focus on the

Figure 4. 75-year-old male with hepatocellular carcinoma undergoing preoperative evaluation. Contrast-enhanced MRI shows a 70 mm lesion with arterial phase hyperenhancement (A, arrow), washout and capsule on portal venous phase (B). Elastography acquired for assessment of liver fibrosis demonstrate a stiffness of 2.2 kPa (C). Lesion stiffness was 2.7 kPa which was consistent with the diagnosis of HCC (D). Resection specimen relieved a moderately differentiated HCC arising in non-cirrhotic liver parenchyma.

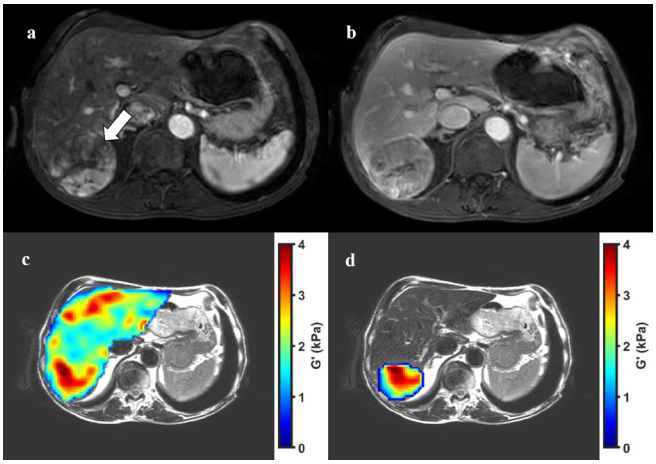

association between viscoelastic tumor properties and intrinsic tumor pressure considered both as a possible indicator of drug resistance, and as a prognostic feature.

Radiomics

Recent studies have explored the potential of MRI-based radiomics for characterization and prognostication in FLLs, with promising results. Initial experiences applied radiomics and texture analysis to T2W MRI for the differentiation of benign and malignant FLLs,[54–56] with an overall classification accuracy of 90.1% in the study by Gatos et al,[55] and 77% in that of Jansen et al.[56] The performance of MRI-based texture features was found to be excellent in benign lesions to differentiate focal nodular hyperplasia from hepatocellular adenoma on gadoxetate-disodium enhanced MRI (AUROC 0.869 [95%CI, 0.777–0.933] for the diagnosis of HCA), with added value compared to hepatobiliary phase hypointensity.[57]

Several radiomic applications have been explored in patients with HCC. Multiple radiomic models extracted from MRI sequences have been shown to be highly accurate in the prediction of the histopathological features of tumor aggressiveness in HCC, such as tumor grade,[58,59] Ki-67 expression (a marker of tumor proliferation),[60] and cytokeratin 19 expression (a marker associated with poor HCC prognosis).[61]

Assessment of tumor response and follow-up

The assessment of tumor response relies on various sets of semi-quantitative criteria that monitor changes of tumor characteristics on imaging over time. Recognized limitations of this approach are the need to wait several weeks (or months) after the initiation of treatments, with subsequent delay in treatment modification in non-responders, and the variety of available criteria, focusing of various tumor features (tumor size, tumor viability, etc.), making it more difficult to compare results. Quantitative imaging aims at addressing these limitations by providing an earlier and more standardized response assessment.

Diffusion-weighted imaging

In a surgical series of small resected HCC (≤5 cm), Lee et al. showed that tumor size ($p = 0.002$) and ADCmin ≤0.773×10^{-3} mm^2/s ($p < 0.001$) were independent risk factors for early HCC recurrence.[62] Pre-clinical and clinical studies have shown that ADC values could indicate the degree of tumor necrosis in HCCs treated with loco-regional therapy as necrotic tissue shows higher ADC values than viable tissue.[63–68] The meta-analysis by Liu et al. including 12 studies comprising 624 patients and 712 tumors reported a pooled sensitivity, specificity and AUROC of DWI in diagnosing residual or recurrent HCCs after TACE of 85% (95%CI: 74–92%), 83% (95%CI: 75–88%), and 0.90 (95%CI: 0.87–0.92), respectively.[69] Interestingly, these alterations can be observed as early as one week after the treatment, thus helping predict further response.[67,68,70] Barat et al. suggested that a low ADC value at 1 month after ablation was associated with an early local recurrence of HCC.[71] Several teams have also investigated the role of the pre-treatment ADC value in predicting tumor response. Although these series are preliminary, tumor ADC obtained before transarterial chemoembolization or radioembolization can be used to predict tumor response and patient survival.[72–74]

In patients with liver metastases, ADC could predict poor response to ablation, radioembolization, or systemic therapies.[75–77] Nevertheless, increase in ADC values in responding liver metastases that occur within days after the start of treatment appear of smaller magnitude than the variability of ADC measurement, suggesting that it is not reliable enough to predict final response at such an early time point in individual lesions.

Intravoxel incoherent motion

One study suggested that D and D* obtained after treatment may be correlated to lipiodol uptake, early response, and progression-free survival in patients undergoing transarterial chemoembolization (TACE) for the treatment of HCC.[78] In a study by Chiaradia et al., D was shown to have a significant positive correlation with the degree of tumor necrosis, but not with that of viable tumor, in resected colorectal hepatic metastases treated with systemic chemotherapy.[43] A prospective study by Kim et al[79] observed significant increase in ADC and D values of hepatic metastases after chemotherapy in responder patients, while no changes were noted in non-responders.

Perfusion imaging

Interesting applications of quantitative MRI perfusion have been investigated for the assessment of HCC, in particular for the monitoring of treatment response after locoregional and systemic therapies.[80] Ippolito et al. used a semi-quantitative perfusion approach and found differences between tumors

with complete and incomplete TACE treatment.[81] This is in line with results published by Taouli et al.[49] Authors were able to observe significantly lower portal venous hepatic blood flow and higher arterial fraction in tumors that were not targeted by chemoembolization, compared to those that were. Unfortunately, these studies did not compare results of perfusion studies with morphological criteria, or used them as reference.

Studies have also evaluated the ability of perfusion MR imaging to document early changes after treatment in order to identify further responders. In the study by Braren et al. using a rodent preclinical model,[82] the quantification of the extravascular extracellular volume fraction (v_e) as soon as one day after trans-arterial embolization was associated with further tumor necrosis. Going one step further, Michielsen et al[83] suggested that pre-TACE perfusion parameters assessed with perfusion MRI could help predict of progression-free survival.

Hsu et al[84] showed that the K^{trans} of advanced HCC was well correlated with tumor response, progression-free survival, and overall survival in patients treated with systemic therapy, suggesting that a reduction in K^{trans} may be related to changes in tumor vascularization after anti angiogenetic therapy. Subsequent studies have supported the value of early perfusion changes in advanced HCC for the prediction of overall survival after systemic treatment.[85,86]

Similar results have been reported with K^{trans} and a variety of perfusion parameters in patients with colorectal metastases treated with chemotherapy in combination with various targeted therapies,. Coenegrachts et al[87] showed that the constant rate between extravascular extracellular space and blood plasma at baseline (*i.e.*, $k_{ep} = K^{trans}/v_e$) was significantly higher in responders than in non-responders. They also showed that responders had a significant decrease in k_{ep} after six weeks of treatment. In the study by De Bruyne et al.,[88] >40% reduction in K^{trans} after treatment was associated with a significantly longer progression-free survival. These may be shown early after treatment introduction, as suggested by Hirashima et al.[89] Authors observed variations in both k_{ep} and K^{trans} within a week after treatment that could help predict response to chemotherapy.

Elastography

Lower tumor stiffness may be associated with greater intralesional necrosis, as observed in HCC treated with locoregional therapies.[90] On the other hand, increased HCC stiffness has been evaluated as a potential predictor of early recurrence after hepatic resection.[91,92] In this setting, high pre-treatment tumor stiffness may be an additional noninvasive biomarker for a poor prognosis in patients with HCC.[93]

Radiomics

Texture-based models have been reported to predict tumor response after TACE[94] and early recurrence after curative hepatectomy, alone or in combination with morphological criteria.[95–97] There has been some research on MRI-based radiomics in hepatic metastases, but further studies are needed to identify the role of this technique in this context.[98]

APPLICATIONS IN CLINICAL PRACTICE: LIMITATIONS AND PERSPECTIVES

Diffusion-weighted imaging

Although ADC quantification has been shown to be applicable to several clinical situations, ADC values still vary significantly (and thus, possible cutoff values) with different MRI scanners.[99–101] Makyarenko et al. used an ice-water phantom and showed a standard deviation of ADC measured across 35 scanners < 2%.[100] The day-to-day repeatability of the measurements was within 4.5%, inter-site reproducibility of ADC was within 3%. Sasaki et al. performed a multivendor, multi-institutional comparison study and reported that, with the exception of one vendor, the intervendor variability at 1.5 T in a clinical setting was as high as 7%. Moreover, there was substantial intra-imager variability, up to 8%, depending on the coil systems in certain imagers.[101] The ADC ratio between lesions and the liver parenchyma has been proposed to overcome some of these limitations, but it should be noted that the ADC of the background liver parenchyma is affected by its quality (for instance by the presence of fibrosis in patients with chronic liver disease). Moreover, DWI sequences are very sensitive to artifacts that can negatively influence image quality and ADC quantification.

At present, assessment of the ADC map for the characterization of FLLs is usually qualitative. Quantitative rules of thumbs, for instance liver metastases and cholangiocarcinoma usually displaying an ADC $\leq 1.0\times10^{-3}$ mm^2/s are rare, explaining why quantitative measurements are not routinely used for patient management or clinical decision making.

Intravoxel incoherent motion

Current clinical applications of IVIM have been limited by several technical factors and the need for specific acquisition protocols.[7] For the moment the added diagnostic value of IVIM analysis compared to the ADC map is still a question because IVIM may be affected by MRI field strength, number or choice of *b*-values, and post-processing calculation models.[102] Particularly, number of *b*-values widely varies in the published studies, with most research using from four to more than ten *b*-values. Although a greater number of *b*-values may provide more accurate information, the acquisition time would significantly increase in clinical practice. These practical limitations as well as a diagnostic performance that is similar to the extensively used ADC map could explain the limited clinical use of this quantitative method in tertiary centers for the assessment of FLLs.

Perfusion imaging

There are several reasons for the limited number of clinical applications of perfusion imaging for FLLs. Differences in imaging systems, technical parameters without standardized acquisition protocols, respiratory motions, and different pharmacokinetic models makes it difficult to compare and validate research studies in FLLs.[3] Also, perfusion quantification requires prospective acquisition with contrast administration

and complex post-processing methods including additional scanning and interpretation time, limiting its use to specialized or tertiary centers. Thus, for the moment, perfusion MR imaging is only used in research settings in specialized centers for the treatment of FLLs.[9] Recent commercially available sequences, such as the golden-angle radial sparse parallel (GRASP) imaging, have been shown to allow for a reliable and robust assessment of hepatic perfusion parameters with quantitative results comparable to perfusion CT.[103] These new generation of sequences is promising in making perfusion data more easily available, together with a routine visual interpretation of contrast enhancement.

Elastography

The routine acquisition of MRE requires specific hardware that is often only available in tertiary centers, and requires additional scanning time. This significantly limits the applicability of MRE for the characterization of FLLs, especially compared to the performance of qualitative assessment by up-to-date contrast-enhanced MRI and other quantitative imaging methods. New transducer-free elastography methods using, for instance, intrinsic cardiac motion appear promising to overcome this limitation.

Radiomics

Although the results of radiomics are promising for the assessment of FLLs, there are still challenges that limit its application in clinical practice. Lack of methodological standardization, time-consuming segmentation, and the type of extracted features with different in-house designed or research-based software have limited the reproducibility of radiomic models.[104] Moreover, radiomic features are affected by acquisition parameters, in particular, slice thickness.[105] Therefore, methodological standardization and reproducibility of features are needed to provide robust radiomic models that can be used in different settings.

BRIDGING THE GAP BETWEEN RESEARCH AND PRACTICE

The current situation of quantitative MRI in FLLs is somewhat paradoxical. We hereby discuss results of numerous studies reporting promising results in a wide variety of clinical settings but very few applications exist in clinical practice. As this review shows, quantitative MRI could theoretically be used in combination with qualitative imaging for the assessment of FLLs and could provide solutions in various clinical scenarios. However, the expected application of these results into routine clinical practice has not occurred.

There are many possible explanations for this. First, quantitative imaging is difficult to perform in the liver because it is a mobile, blood-filled, flexible organ with dual vascular input and fenestrated sinusoids. This requires advanced registration techniques and complex microvascular or tissue models. Second, patients have different morphotypes, capacities to hold their breath, possible iron overload, as well as fasting states. Third, MRI sequences are patented or trademarked making direct comparison difficult. Furthermore, the MRI signal is affected by the magnetic field strength and the overall architecture of machines and antennas. Moreover, most of the published studies are single center and retrospective, without standardized acquisition parameters, post-processing methods or predicted outcome. This results in significant intra- and inter-vendor, software, reader, and patient variability, as discussed above. Observed statistical differences in populations are, therefore, rarely applicable to individuals. There are also still concerns about the need for additional scanning time and the complexity of imaging interpretation. Finally, the good to excellent performance of qualitative imaging with up-to-date MR protocols, and easy access to percutaneous biopsy narrows the number of unmet needs that quantitative imaging can address.

Overcoming these limitations will require a significant collective effort. Nevertheless, the medical imaging community has never been more aware of this and has never had more powerful tools to succeed, as illustrated by initiatives such as the Quantitative Imaging Biomarkers Alliance or the Radiological Society of North America[106] or the Biomarker Inventory or the European Society of Radiology.[107]

REFERENCES

1. Donato H, França M, Candelária I, Caseiro-Alves F. Liver MRI: from basic protocol to advanced techniques. *Eur J Radiol* 2017; **93**: 30–9. doi: https://doi.org/10.1016/j.ejrad.2017.05.028
2. Taouli B, Koh D-M. Diffusion-Weighted MR imaging of the liver. *Radiology* 2010; **254**: 47–66. doi: https://doi.org/10.1148/radiol.09090021
3. Chandarana H, Taouli B. Diffusion and perfusion imaging of the liver. *Eur J Radiol* 2010; **76**: 348–58. doi: https://doi.org/10.1016/j.ejrad.2010.03.016
4. Ronot M, Clift AK, Vilgrain V, Frilling A. Functional imaging in liver tumours. *J Hepatol* 2016; **65**: 1017–30. doi: https://doi.org/10.1016/j.jhep.2016.06.024
5. Guiu B, Cercueil J-P. Liver diffusion-weighted MR imaging: the Tower of Babel? *Eur Radiol* 2011; **21**: 463–7. doi: https://doi.org/10.1007/s00330-010-2017-y
6. Duran R, Ronot M, Kerbaol A, Van Beers B, Vilgrain V. Hepatic hemangiomas: factors associated with T2 shine-through effect on diffusion-weighted Mr sequences. *Eur J Radiol* 2014; **83**: 468–78. doi: https://doi.org/10.1016/j.ejrad.2013.11.023
7. Koh D-M, Collins DJ, Orton MR. Intravoxel incoherent motion in body diffusion-weighted MRI: reality and challenges. *AJR Am J Roentgenol* 2011; **196**: 1351–61. doi: https://doi.org/10.2214/AJR.10.5515
8. Le Bihan D, Breton E, Lallemand D, Aubin ML, Vignaud J, Laval-Jeantet M. Separation of diffusion and perfusion in intravoxel incoherent motion MR imaging. *Radiology* 1988; **168**: 497–505. doi: https://doi.org/10.1148/radiology.168.2.3393671

9. Ronot M, Lambert S, Daire J-L, Lagadec M, Doblas S, Garteiser P, et al. Can we justify not doing liver perfusion imaging in 2013? *Diagn Interv Imaging* 2013; **94**: 1323–36. doi: https://doi.org/10.1016/j.diii.2013.06.005
10. Kanematsu M, Goshima S, Watanabe H, Kondo H, Kawada H, Noda Y, et al. Diffusion/perfusion MR imaging of the liver: practice, challenges, and future. *Magn Reson Med Sci* 2012; **11**: 151–61. doi: https://doi.org/10.2463/mrms.11.151
11. Hectors SJ, Wagner M, Besa C, Bane O, Dyvorne HA, Fiel MI, et al. Intravoxel incoherent motion diffusion-weighted imaging of hepatocellular carcinoma: is there a correlation with flow and perfusion metrics obtained with dynamic contrast-enhanced MRI? *J Magn Reson Imaging* 2016; **44**: 856–64. doi: https://doi.org/10.1002/jmri.25194
12. Tofts PS, Brix G, Buckley DL, Evelhoch JL, Henderson E, Knopp MV, et al. Estimating kinetic parameters from dynamic contrast-enhanced T(1)-weighted MRI of a diffusable tracer: standardized quantities and symbols. *J Magn Reson Imaging* 1999; **10**: 223–32. doi: https://doi.org/10.1002/(SICI)1522-2586(199909)10:3<223::AID-JMRI2>3.0.CO;2-S
13. Venkatesh SK, Yin M, Ehman RL. Magnetic resonance elastography of liver: technique, analysis, and clinical applications. *J Magn Reson Imaging* 2013; **37**: 544–55. doi: https://doi.org/10.1002/jmri.23731
14. Guglielmo FF, Venkatesh SK, Mitchell DG. Liver Mr elastography technique and image interpretation: pearls and pitfalls. *Radiographics* 2019; **39**: 1983–2002. doi: https://doi.org/10.1148/rg.2019190034
15. Gillies RJ, Kinahan PE, Hricak H. Radiomics: images are more than pictures, they are data. *Radiology* 2016; **278**: 563–77. doi: https://doi.org/10.1148/radiol.2015151169
16. Vernuccio F, Cannella R, Comelli A, Salvaggio G, Lagalla R, Midiri M. Radiomica e intelligenza artificiale: nuove frontiere in medicina [Radiomics and artificial intelligence: new frontiers in medicine. *Recenti Prog Med* 2020; **111**: 130–5.
17. Baeßler B, Weiss K, Pinto Dos Santos D. Robustness and reproducibility of Radiomics in magnetic resonance imaging: a phantom study. *Invest Radiol* 2019; **54**: 221–8. doi: https://doi.org/10.1097/RLI.0000000000000530
18. Miranda Magalhaes Santos JM, Clemente Oliveira B, Araujo-Filho JdeAB, Assuncao-Jr AN, de M. Machado FA, Carlos Tavares Rocha C, et al. State-Of-The-Art in radiomics of hepatocellular carcinoma: a review of basic principles, applications, and limitations. *Abdom Radiol* 2020; **45**: 342–53. doi: https://doi.org/10.1007/s00261-019-02299-3
19. Lewis S, Hectors S, Taouli B. Radiomics of hepatocellular carcinoma. *Abdom Radiol* 2020;.
20. Parikh T, Drew SJ, Lee VS, Wong S, Hecht EM, Babb JS, et al. Focal liver lesion detection and characterization with diffusion-weighted MR imaging: comparison with standard breath-hold T2-weighted imaging. *Radiology* 2008; **246**: 812–22. doi: https://doi.org/10.1148/radiol.2463070432
21. Agnello F, Ronot M, Valla DC, Sinkus R, Van Beers BE, Vilgrain V. High-b-value diffusion-weighted MR imaging of benign hepatocellular lesions: quantitative and qualitative analysis. *Radiology* 2012; **262**: 511–9. doi: https://doi.org/10.1148/radiol.11110922
22. Pankaj Jain T, Kan WT, Edward S, Fernon H, Kansan Naider R. Evaluation of ADC_{ratio} on liver MRI diffusion to discriminate benign versus malignant solid liver lesions. *Eur J Radiol Open* 2018; **5**: 209–14. doi: https://doi.org/10.1016/j.ejro.2018.10.002
23. Inchingolo R, De Gaetano AM, Curione D, Ciresa M, Miele L, Pompili M, et al. Role of diffusion-weighted imaging, apparent diffusion coefficient and correlation with hepatobiliary phase findings in the differentiation of hepatocellular carcinoma from dysplastic nodules in cirrhotic liver. *Eur Radiol* 2015; **25**: 1087–96. doi: https://doi.org/10.1007/s00330-014-3500-7
24. Heo SH, Jeong YY, Shin SS, Kim JW, Lim HS, Lee JH, et al. Apparent diffusion coefficient value of diffusion-weighted imaging for hepatocellular carcinoma: correlation with the histologic differentiation and the expression of vascular endothelial growth factor. *Korean J Radiol* 2010; **11**: 295–303. doi: https://doi.org/10.3348/kjr.2010.11.3.295
25. Li X, Zhang K, Shi Y, Wang F, Meng X. Correlations between the minimum and mean apparent diffusion coefficient values of hepatocellular carcinoma and tumor grade. *J Magn Reson Imaging* 2016; **44**: 1442–7. doi: https://doi.org/10.1002/jmri.25323
26. Ogihara Y, Kitazume Y, Iwasa Y, Taura S, Himeno Y, Kimura T, et al. Prediction of histological grade of hepatocellular carcinoma using quantitative diffusion-weighted MRI: a retrospective multivendor study. *Br J Radiol* 2018; **91**: 20170728. doi: https://doi.org/10.1259/bjr.20170728
27. Zhao J, Li X, Zhang K, Yin X, Meng X, Han L, et al. Prediction of microvascular invasion of hepatocellular carcinoma with preoperative diffusion-weighted imaging: a comparison of mean and minimum apparent diffusion coefficient values. *Medicine* 2017; **96**: e7754. doi: https://doi.org/10.1097/MD.0000000000007754
28. Ichikawa S, Motosugi U, Ichikawa T, Sano K, Morisaka H, Araki T. Intravoxel incoherent motion imaging of focal hepatic lesions. *J Magn Reson Imaging* 2013; **37**: 1371–6. doi: https://doi.org/10.1002/jmri.23930
29. Luo M, Zhang L, Jiang X-H, Zhang W-D. Intravoxel incoherent motion diffusion-weighted imaging: evaluation of the differentiation of solid hepatic lesions. *Transl Oncol* 2017; **10**: 831–8. doi: https://doi.org/10.1016/j.tranon.2017.08.003
30. Wu H, Liang Y, Jiang X, Wei X, Liu Y, Liu W, et al. Meta-Analysis of intravoxel incoherent motion magnetic resonance imaging in differentiating focal lesions of the liver. *Medicine* 2018; **97**: e12071. doi: https://doi.org/10.1097/MD.0000000000012071
31. Watanabe H, Kanematsu M, Goshima S, Kajita K, Kawada H, Noda Y, et al. Characterizing focal hepatic lesions by free-breathing intravoxel incoherent motion MRI at 3.0 T. *Acta Radiol* 2014; **55**: 1166–73. doi: https://doi.org/10.1177/0284185113514966
32. Noda Y, Goshima S, Fujimoto K, Akamine Y, Kajita K, Kawai N, et al. Comparison of the diagnostic value of mono-exponential, Bi-exponential, and stretched exponential signal models in diffusion-weighted MR imaging for differentiating benign and malignant hepatic lesions. *Magn Reson Med Sci* 2021; **20**: 69–75. doi: https://doi.org/10.2463/mrms.mp.2019-0151
33. Choi IY, Lee SS, Sung YS, Cheong H, Lee H, Byun JH, et al. Intravoxel incoherent motion diffusion-weighted imaging for characterizing focal hepatic lesions: correlation with lesion enhancement. *J Magn Reson Imaging* 2017; **45**: 1589–98. doi: https://doi.org/10.1002/jmri.25492
34. Kim HC, Seo N, Chung YE, Park M-S, Choi J-Y, Kim M-J. Characterization of focal liver lesions using the stretched exponential model: comparison with monoexponential and biexponential diffusion-weighted magnetic resonance imaging. *Eur Radiol* 2019; **29**: 5111–20. doi: https://doi.org/10.1007/s00330-019-06048-4
35. Wagner M, Doblas S, Daire J-L, Paradis V, Haddad N, Leitão H, et al. Diffusion-Weighted MR imaging for the regional characterization of liver tumors. *Radiology* 2012; **264**: 464–72. doi: https://doi.org/10.1148/radiol.12111530

36. Granata V, Fusco R, Catalano O, Guarino B, Granata F, Tatangelo F, et al. Intravoxel incoherent motion (IVIM) in diffusion-weighted imaging (DWI) for hepatocellular carcinoma: correlation with histologic grade. *Oncotarget* 2016; **7**: 79357–64. doi: https://doi.org/10.18632/oncotarget.12689
37. Ichikawa S, Motosugi U, Hernando D, Morisaka H, Enomoto N, Matsuda M, et al. Histological grading of hepatocellular carcinomas with Intravoxel incoherent motion diffusion-weighted imaging: inconsistent results depending on the fitting method. *Magn Reson Med Sci* 2018; **17**: 168–73. doi: https://doi.org/10.2463/mrms.mp.2017-0047
38. Woo S, Lee JM, Yoon JH, Joo I, Han JK, Choi BI. Intravoxel incoherent motion diffusion-weighted MR imaging of hepatocellular carcinoma: correlation with enhancement degree and histologic grade. *Radiology* 2014; **270**: 758–67. doi: https://doi.org/10.1148/radiol.13130444
39. Yang D, She H, Wang X, Yang Z, Wang Z. Diagnostic accuracy of quantitative diffusion parameters in the pathological grading of hepatocellular carcinoma: a meta-analysis. *J Magn Reson Imaging* 2020; **51**: 1581–93. doi: https://doi.org/10.1002/jmri.26963
40. Zhao W, Liu W, Liu H, Yi X, Hou J, Pei Y, et al. Preoperative prediction of microvascular invasion of hepatocellular carcinoma with IVIM diffusion-weighted MR imaging and Gd-EOB-DTPA-enhanced MR imaging. *PLoS One* 2018; **13**: e0197488. doi: https://doi.org/10.1371/journal.pone.0197488
41. Wei Y, Huang Z, Tang H, Deng L, Yuan Y, Li J, et al. IVIM improves preoperative assessment of microvascular invasion in HCC. *Eur Radiol* 2019; **29**: 5403–14. doi: https://doi.org/10.1007/s00330-019-06088-w
42. Granata V, Fusco R, Risi C, Ottaiano A, Avallone A, De Stefano A, et al. Diffusion-Weighted MRI and diffusion Kurtosis imaging to detect Ras mutation in colorectal liver metastasis. *Cancers* 2020; **12**: 2420. doi: https://doi.org/10.3390/cancers12092420
43. Chiaradia M, Baranes L, Van Nhieu JT, Vignaud A, Laurent A, Decaens T, et al. Intravoxel incoherent motion (IVIM) MR imaging of colorectal liver metastases: are we only looking at tumor necrosis? *J Magn Reson Imaging* 2014; **39**: 317–25. doi: https://doi.org/10.1002/jmri.24172
44. Chen J, Si Y, Zhao K, Shi X, Bi W, Liu S-E, et al. Evaluation of quantitative parameters of dynamic contrast-enhanced magnetic resonance imaging in qualitative diagnosis of hepatic masses. *BMC Med Imaging* 2018; **18**: 56. doi: https://doi.org/10.1186/s12880-018-0299-8
45. Alicioglu B, Guler O, Bulakbasi N, Akpinar S, Tosun O, Comunoglu C. Utility of semiquantitative parameters to differentiate benign and malignant focal hepatic lesions. *Clin Imaging* 2013; **37**: 692–6. doi: https://doi.org/10.1016/j.clinimag.2013.01.012
46. Pahwa S, Liu H, Chen Y, Dastmalchian S, O'Connor G, Lu Z, et al. Quantitative perfusion imaging of neoplastic liver lesions: a multi-institution study. *Sci Rep* 2018; **8**: 4990. doi: https://doi.org/10.1038/s41598-018-20726-1
47. Ghodasara S, Pahwa S, Dastmalchian S, Gulani V, Chen Y. Free-Breathing 3D liver perfusion quantification using a Dual-Input two-compartment model. *Sci Rep* 2017; **7**: 17502. doi: https://doi.org/10.1038/s41598-017-17753-9
48. Koh TS, Thng CH, Hartono S, Kwek JW, Khoo JBK, Miyazaki K, et al. Dynamic contrast-enhanced MRI of neuroendocrine hepatic metastases: a feasibility study using a dual-input two-compartment model. *Magn Reson Med* 2011; **65**: 250–60. doi: https://doi.org/10.1002/mrm.22596
49. Taouli B, Johnson RS, Hajdu CH, Oei MTH, Merad M, Yee H, et al. Hepatocellular carcinoma: perfusion quantification with dynamic contrast-enhanced MRI. *AJR Am J Roentgenol* 2013; **201**: 795–800. doi: https://doi.org/10.2214/AJR.12.9798
50. Totman JJ, O'gorman RL, Kane PA, Karani JB. Comparison of the hepatic perfusion index measured with gadolinium-enhanced volumetric MRI in controls and in patients with colorectal cancer. *Br J Radiol* 2005; **78**: 105–9. doi: https://doi.org/10.1259/bjr/13525061
51. Venkatesh SK, Yin M, Glockner JF, Takahashi N, Araoz PA, Talwalkar JA, et al. Mr elastography of liver tumors: preliminary results. *AJR Am J Roentgenol* 2008; **190**: 1534–40. doi: https://doi.org/10.2214/AJR.07.3123
52. Garteiser P, Doblas S, Daire J-L, Wagner M, Leitao H, Vilgrain V, et al. Mr elastography of liver tumours: value of viscoelastic properties for tumour characterisation. *Eur Radiol* 2012; **22**: 2169–77. doi: https://doi.org/10.1007/s00330-012-2474-6
53. Thompson SM, Wang J, Chandan VS, Glaser KJ, Roberts LR, Ehman RL, et al. Mr elastography of hepatocellular carcinoma: correlation of tumor stiffness with histopathology features-Preliminary findings. *Magn Reson Imaging* 2017; **37**: 41–5. doi: https://doi.org/10.1016/j.mri.2016.11.005
54. Mayerhoefer ME, Schima W, Trattnig S, Pinker K, Berger-Kulemann V, Ba-Ssalamah A. Texture-based classification of focal liver lesions on MRI at 3.0 Tesla: a feasibility study in cysts and hemangiomas. *J Magn Reson Imaging* 2010; **32**: 352–9. doi: https://doi.org/10.1002/jmri.22268
55. Gatos I, Tsantis S, Karamesini M, Spiliopoulos S, Karnabatidis D, Hazle JD, et al. Focal liver lesions segmentation and classification in nonenhanced T2-weighted MRI. *Med Phys* 2017; **44**: 3695–705. doi: https://doi.org/10.1002/mp.12291
56. Jansen MJA, Kuijf HJ, Veldhuis WB, Wessels FJ, Viergever MA, Pluim JPW. Automatic classification of focal liver lesions based on MRI and risk factors. *PLoS One* 2019; **14**: e0217053. doi: https://doi.org/10.1371/journal.pone.0217053
57. Cannella R, Rangaswamy B, Minervini MI, Borhani AA, Tsung A, Furlan A. Value of texture analysis on gadoxetic acid-enhanced MRI for differentiating hepatocellular adenoma from focal nodular hyperplasia. *AJR Am J Roentgenol* 2019; **212**: 538–46. doi: https://doi.org/10.2214/AJR.18.20182
58. Wu M, Tan H, Gao F, Hai J, Ning P, Chen J, et al. Predicting the grade of hepatocellular carcinoma based on non-contrast-enhanced MRI radiomics signature. *Eur Radiol* 2019; **29**: 2802–11. doi: https://doi.org/10.1007/s00330-018-5787-2
59. Feng M, Zhang M, Liu Y, Jiang N, Meng Q, Wang J, et al. Texture analysis of Mr images to identify the differentiated degree in hepatocellular carcinoma: a retrospective study. *BMC Cancer* 2020; **20**: 611. doi: https://doi.org/10.1186/s12885-020-07094-8
60. Li Y, Yan C, Weng S, Shi Z, Sun H, Chen J, et al. Texture analysis of multi-phase MRI images to detect expression of Ki67 in hepatocellular carcinoma. *Clin Radiol* 2019; **74**: 813.e19–813.e27. doi: https://doi.org/10.1016/j.crad.2019.06.024
61. Wang H-Q, Yang C, Zeng M-S, Rao S-X, Ji Y, Weng X, et al. Magnetic resonance texture analysis for the identification of cytokeratin 19-positive hepatocellular carcinoma. *Eur J Radiol* 2019; **117**: 164–70. doi: https://doi.org/10.1016/j.ejrad.2019.06.016
62. Lee S, Kim SH, Hwang JA, Lee JE, Ha SY. Pre-Operative ADC predicts early recurrence of HCC after curative resection. *Eur Radiol* 2019; **29**: 1003–12. doi: https://doi.org/10.1007/s00330-018-5642-5
63. Mannelli L, Kim S, Hajdu CH, Babb JS, Clark TWI, Taouli B. Assessment of tumor necrosis of hepatocellular carcinoma after chemoembolization: diffusion-weighted and contrast-enhanced MRI with histopathologic correlation of the explanted

liver. *AJR Am J Roentgenol* 2009; **193**: 1044–52. doi: https://doi.org/10.2214/AJR.08.1461
64. Namimoto T, Yamashita Y, Sumi S, Tang Y, Takahashi M. Focal liver masses: characterization with diffusion-weighted echo-planar MR imaging. *Radiology* 1997; **204**: 739–44. doi: https://doi.org/10.1148/radiology.204.3.9280252
65. Bonekamp S, Jolepalem P, Lazo M, Gulsun MA, Kiraly AP, Kamel IR. Hepatocellular carcinoma: response to TACE assessed with semiautomated volumetric and functional analysis of diffusion-weighted and contrast-enhanced MR imaging data. *Radiology* 2011; **260**: 752–61. doi: https://doi.org/10.1148/radiol.11102330
66. Yuan Z, Zhang J, Yang H, Ye X-D, Xu L-C, Li W-T, , LC X, WT L. Diffusion-Weighted MR imaging of hepatocellular carcinoma: current value in clinical evaluation of tumor response to locoregional treatment. *J Vasc Interv Radiol* 2016; **27**: 20–30. doi: https://doi.org/10.1016/j.jvir.2015.10.003
67. Kamel IR, Liapi E, Reyes DK, Zahurak M, Bluemke DA, Geschwind J-FH. Unresectable hepatocellular carcinoma: serial early vascular and cellular changes after transarterial chemoembolization as detected with MR imaging. *Radiology* 2009; **250**: 466–73. doi: https://doi.org/10.1148/radiol.2502072222
68. Chen C-Y, Li C-W, Kuo Y-T, Jaw T-S, Wu D-K, Jao J-C, CW L, , et al. Early response of hepatocellular carcinoma to transcatheter arterial chemoembolization: choline levels and MR diffusion constants--initial experience. *Radiology* 2006; **239**: 448–56. doi: https://doi.org/10.1148/radiol.2392042202
69. Liu Z, Fan J-M, He C, Li Z-F, Xu Y-S, Li Z, et al. Utility of diffusion weighted imaging with the quantitative apparent diffusion coefficient in diagnosing residual or recurrent hepatocellular carcinoma after transarterial chemoembolization: a meta-analysis. *Cancer Imaging* 2020; **20**: 3. doi: https://doi.org/10.1186/s40644-019-0282-9
70. Chung JC, Naik NK, Lewandowski RJ, Deng J, Mulcahy MF, Kulik LM, et al. Diffusion-Weighted magnetic resonance imaging to predict response of hepatocellular carcinoma to chemoembolization. *World J Gastroenterol* 2010; **16**: 3161–7. doi: https://doi.org/10.3748/wjg.v16.i25.3161
71. Barat M, Fohlen A, Cassinotto C, Jannot AS, Dautry R, Pelage J-P, et al. One-month apparent diffusion coefficient correlates with response to radiofrequency ablation of hepatocellular carcinoma. *J Magn Reson Imaging* 2017; **45**: 1648–58. doi: https://doi.org/10.1002/jmri.25521
72. Mannelli L, Kim S, Hajdu CH, Babb JS, Taouli B. Serial diffusion-weighted MRI in patients with hepatocellular carcinoma: prediction and assessment of response to transarterial chemoembolization. preliminary experience. *Eur J Radiol* 2013; **82**: 577–82. doi: https://doi.org/10.1016/j.ejrad.2012.11.026
73. Dong S, Ye X-D, Yuan Z, Xu L-C, Xiao X-S, XD Y, . Relationship of apparent diffusion coefficient to survival for patients with unresectable primary hepatocellular carcinoma after chemoembolization. *Eur J Radiol* 2012; **81**: 472–7. doi: https://doi.org/10.1016/j.ejrad.2010.12.081
74. Kokabi N, Camacho JC, Xing M, Qiu D, Kitajima H, Mittal PK, et al. Apparent diffusion coefficient quantification as an early imaging biomarker of response and predictor of survival following yttrium-90 radioembolization for unresectable infiltrative hepatocellular carcinoma with portal vein thrombosis. *Abdom Imaging* 2014; **39**: 969–78. doi: https://doi.org/10.1007/s00261-014-0127-8
75. Szurowska E, Nowicki TK, Izycka-Swieszewska E, Zadrozny D, Markiet K, Studniarek M. Predictive value of apparent diffusion coefficient in evaluation of colorectal carcinoma hepatic metastases' response to radiofrequency ablation. *J Magn Reson Imaging* 2013; **38**: 1027–32. doi: https://doi.org/10.1002/jmri.24089
76. Alis D, Durmaz ESM, Gulsen F, Bas A, Kabasakal L, Sager S, et al. Prognostic value of ADC measurements in predicting overall survival in patients undergoing ^{90}Y radioembolization for colorectal cancer liver metastases. *Clin Imaging* 2019; **57**: 124–30. doi: https://doi.org/10.1016/j.clinimag.2019.05.015
77. Deckers F, De Foer B, Van Mieghem F, Botelberge T, Weytjens R, Padhani A, et al. Apparent diffusion coefficient measurements as very early predictive markers of response to chemotherapy in hepatic metastasis: a preliminary investigation of reproducibility and diagnostic value. *J Magn Reson Imaging* 2014; **40**: 448–56. doi: https://doi.org/10.1002/jmri.24359
78. Park YS, Lee CH, Kim JH, Kim IS, Kiefer B, Seo TS, et al. Using intravoxel incoherent motion (IVIM) MR imaging to predict lipiodol uptake in patients with hepatocellular carcinoma following transcatheter arterial chemoembolization: a preliminary result. *Magn Reson Imaging* 2014; **32**: 638–46. doi: https://doi.org/10.1016/j.mri.2014.03.003
79. Kim JH, Joo I, Kim T-Y, Han S-W, Kim YJ, Lee JM, et al. Diffusion-Related MRI parameters for assessing early treatment response of liver metastases to cytotoxic therapy in colorectal cancer. *AJR Am J Roentgenol* 2016; **207**: W26–32. doi: https://doi.org/10.2214/AJR.15.15683
80. Campos M, Candelária I, Papanikolaou N, Simão A, Ferreira C, Manikis GC, et al. Perfusion magnetic resonance as a biomarker for Sorafenib-Treated advanced hepatocellular carcinoma: a pilot study. *GE Port J Gastroenterol* 2019; **26**: 260–7. doi: https://doi.org/10.1159/000493351
81. Ippolito D, Trattenero C, Talei Franzesi C, Casiraghi A, Lombardi S, Vacirca F, et al. Dynamic contrast-enhanced magnetic resonance imaging with gadolinium Ethoxybenzyl Diethylenetriamine pentaacetic acid for quantitative assessment of vascular effects on Hepatocellular-Carcinoma lesions treated by transarterial chemoembolization or radiofrequency ablation. *J Comput Assist Tomogr* 2016; **40**: 692–700. doi: https://doi.org/10.1097/RCT.0000000000000427
82. Braren R, Altomonte J, Settles M, Neff F, Esposito I, Ebert O, et al. Validation of preclinical multiparametric imaging for prediction of necrosis in hepatocellular carcinoma after embolization. *J Hepatol* 2011; **55**: 1034–40. doi: https://doi.org/10.1016/j.jhep.2011.01.049
83. Michielsen K, De Keyzer F, Verslype C, Dymarkowski S, van Malenstein H, Oyen R, Maleux G, et al. Pretreatment DCE-MRI for prediction of pfs in patients with inoperable HCC treated with TACE. *Cancer Imaging* 2011; **11**(1A): S114. doi: https://doi.org/10.1102/1470-7330.2011.9058
84. Hsu C-Y, Shen Y-C, Yu C-W, Hsu C, Hu F-C, Hsu C-H, CW Y, , Hsu CH, et al. Dynamic contrast-enhanced magnetic resonance imaging biomarkers predict survival and response in hepatocellular carcinoma patients treated with sorafenib and metronomic Tegafur/Uracil. *J Hepatol* 2011; **55**: 858–65. doi: https://doi.org/10.1016/j.jhep.2011.01.032
85. Kim KA, Park M-S, Ji H-J, Park JY, Han K-H, Kim M-J, et al. Diffusion and perfusion MRI prediction of progression-free survival in patients with hepatocellular carcinoma treated with concurrent chemoradiotherapy. *J Magn Reson Imaging* 2014; **39**: 286–92. doi: https://doi.org/10.1002/jmri.24161
86. Chen B-B, Hsu C-Y, Yu C-W, Liang P-C, Hsu C, Hsu C-H, CW Y, Hsu CH, et al. Early perfusion changes within 1 week of systemic treatment measured by

dynamic contrast-enhanced MRI may predict survival in patients with advanced hepatocellular carcinoma. *Eur Radiol* 2017; **27**: 3069–79. doi: https://doi.org/10.1007/s00330-016-4670-2

87. Coenegrachts K, Bols A, Haspeslagh M, Rigauts H. Prediction and monitoring of treatment effect using T1-weighted dynamic contrast-enhanced magnetic resonance imaging in colorectal liver metastases: potential of whole tumour Roi and selective Roi analysis. *Eur J Radiol* 2012; **81**: 3870–6. doi: https://doi.org/10.1016/j.ejrad.2012.07.022
88. De Bruyne S, Van Damme N, Smeets P, Ferdinande L, Ceelen W, Mertens J, et al. Value of DCE-MRI and FDG-PET/CT in the prediction of response to preoperative chemotherapy with bevacizumab for colorectal liver metastases. *Br J Cancer* 2012; **106**: 1926–33. doi: https://doi.org/10.1038/bjc.2012.184
89. Hirashima Y, Yamada Y, Tateishi U, Kato K, Miyake M, Horita Y, et al. Pharmacokinetic parameters from 3-tesla DCE-MRI as surrogate biomarkers of antitumor effects of bevacizumab plus FOLFIRI in colorectal cancer with liver metastasis. *Int J Cancer* 2012; **130**: 2359–65. doi: https://doi.org/10.1002/ijc.26282
90. Gordic S, Ayache JB, Kennedy P, Besa C, Wagner M, Bane O, et al. Value of tumor stiffness measured with Mr elastography for assessment of response of hepatocellular carcinoma to locoregional therapy. *Abdom Radiol* 2017; **42**: 1685–94. doi: https://doi.org/10.1007/s00261-017-1066-y
91. Wang J, Shan Q, Liu Y, Yang H, Kuang S, He B, et al. 3D Mr elastography of hepatocellular carcinomas as a potential biomarker for predicting tumor recurrence. *J Magn Reson Imaging* 2019; **49**: 719–30. doi: https://doi.org/10.1002/jmri.26250
92. Park S-J, Yoon JH, Lee DH, Lim WH, Lee JM. Tumor stiffness measurements on Mr elastography for single nodular hepatocellular carcinomas can predict tumor recurrence after hepatic resection. *J Magn Reson Imaging* 2021; **53**: 587-596. doi: https://doi.org/10.1002/jmri.27359
93. Kim B, Kim SS, Cho SW, Cheong JY, Huh J, Kim JK, et al. Liver stiffness in magnetic resonance elastography is prognostic for sorafenib-treated advanced hepatocellular carcinoma. *Eur Radiol* 2021; **31**: 2507–17. doi: https://doi.org/10.1007/s00330-020-07357-9
94. Yu JY, Zhang HP, Tang ZY, Zhou J, He XJ, Liu YY, et al. Value of texture analysis based on enhanced MRI for predicting an early therapeutic response to transcatheter arterial chemoembolisation combined with high-intensity focused ultrasound treatment in hepatocellular carcinoma. *Clin Radiol* 2018; **73**: 758.e9–758.e18. doi: https://doi.org/10.1016/j.crad.2018.04.013
95. Ahn SJ, Kim JH, Park SJ, Kim ST, Han JK. Hepatocellular carcinoma: preoperative gadoxetic acid-enhanced MR imaging can predict early recurrence after curative resection using image features and texture analysis. *Abdom Radiol* 2019; **44**: 539–48. doi: https://doi.org/10.1007/s00261-018-1768-9
96. Hui TCH, Chuah TK, Low HM, Tan CH. Predicting early recurrence of hepatocellular carcinoma with texture analysis of preoperative MRI: a radiomics study. *Clin Radiol* 2018; **73**: 1056.e11–1056.e16. doi: https://doi.org/10.1016/j.crad.2018.07.109
97. Zhao Y, Wu J, Zhang Q, Hua Z, Qi W, Wang N, et al. Radiomics analysis based on multiparametric MRI for predicting early recurrence in hepatocellular carcinoma after partial hepatectomy. *J Magn Reson Imaging* 2021; **53**: 1066-1079. doi: https://doi.org/10.1002/jmri.27424
98. Zhang H, Li W, Hu F, Sun Y, Hu T, Tong T. Mr texture analysis: potential imaging biomarker for predicting the chemotherapeutic response of patients with colorectal liver metastases. *Abdom Radiol* 2019; **44**: 65–71. doi: https://doi.org/10.1007/s00261-018-1682-1
99. Pathak R, Ragheb H, Thacker NA, Morris DM, Amiri H, Kuijer J, et al. A data-driven statistical model that estimates measurement uncertainty improves interpretation of ADC reproducibility: a multi-site study of liver metastases. *Sci Rep* 2017; **7**: 14084. doi: https://doi.org/10.1038/s41598-017-14625-0
100. Malyarenko D, Galbán CJ, Londy FJ, Meyer CR, Johnson TD, Rehemtulla A, et al. Multi-System repeatability and reproducibility of apparent diffusion coefficient measurement using an ice-water phantom. *J Magn Reson Imaging* 2013; **37**: 1238–46. doi: https://doi.org/10.1002/jmri.23825
101. Sasaki M, Yamada K, Watanabe Y, Matsui M, Ida M, Fujiwara S. Acute stroke imaging standardization Group-Japan (ASIST-Japan) Investigators. variability in absolute apparent diffusion coefficient values across different platforms may be substantial: a multivendor, multi-institutional comparison study. *Radiology* 2008; **249**: 624–30.
102. Li YT, Cercueil J-P, Yuan J, Chen W, Loffroy R, Wáng YXJ. Liver intravoxel incoherent motion (IVIM) magnetic resonance imaging: a comprehensive review of published data on normal values and applications for fibrosis and tumor evaluation. *Quant Imaging Med Surg* 2017; **7**: 59–78. doi: https://doi.org/10.21037/qims.2017.02.03
103. Weiss J, Ruff C, Grosse U, Grözinger G, Horger M, Nikolaou K, et al. Assessment of hepatic perfusion using GRASP MRI: bringing liver MRI on a new level. *Invest Radiol* 2019; **54**: 737–43. doi: https://doi.org/10.1097/RLI.0000000000000586
104. van Timmeren JE, Cester D, Tanadini-Lang S, Alkadhi H, Baessler B. Radiomics in medical imaging—"how-to" guide and critical reflection. *Insights Imaging* 2020; **11**: 91. doi: https://doi.org/10.1186/s13244-020-00887-2
105. Meyer M, Ronald J, Vernuccio F, Nelson RC, Ramirez-Giraldo JC, Solomon J, et al. Reproducibility of CT radiomic features within the same patient: influence of radiation dose and CT reconstruction settings. *Radiology* 2019; **293**: 583–91. doi: https://doi.org/10.1148/radiol.2019190928
106. Quantitative Imaging Biomarkers Alliance. 2021. Available from: https://www.rsna.org/en/research/quantitative-imaging-biomarkers-alliance.
107. Biomarker Inventory.. Available from: https://www.myesr.org/research/biomarkers-inventory [Accessed February 1, 2021].